PHYSICAL REVIEW B VOLUME 54, NUMBER 19 15 NOVEMBER 1996-I

First-principles study of a tilt grain boundary in rutile

I. Dawson and P. D. Bristowe
Department of Materials Science and Metallurgy, University of Cambridge, Pembroke Street, Cambridge, CB2 3QZ, United Kingdom

M.-H. Lee,* M. C. Payne, M. D. Segall, and J. A. White
TCM Group, Cavendish Laboratory, Madingley Road, Cambridge, CB3 OHE, United Kingdom
(Received 26 April 1996; revised manuscript received 25 July 1996)

The atomic and electronic structure of a tilt grain boundary in rutile TiO_2 has been calculated in an *ab initio* manner. The method employs a plane-wave basis set and optimized pseudopotentials and is carried out within the local-density approximation of density-functional theory. The study focuses on the structure and energy of the $\Sigma=15$ 36.9° (210)[001] tilt boundary, which is relaxed to equilibrium using a conjugate gradients iterative minimization technique. The calculations confirm the stability of a proposed atomic model for the boundary and provide some insight into its electronic structure. [S0163-1829(96)08444-5]

I. INTRODUCTION

Rutile TiO_2 is a ceramic semiconductor that displays some useful physical properties that can be exploited in various electrochemical and device applications. It is well known as an opacifying pigment in paints, fabric, and paper but can also be used as a gas and humidity sensor and as a low voltage surge protector.[1,2] In this paper we focus on the material's electronic rather than optical properties and view it as a model semiconducting oxide upon which first principles calculations can be performed. In the application of TiO_2 as a surge protector (a varistor), the operation and efficiency of the device is critically dependent on the microstructure and chemistry of the material and, in particular, on the presence of internal interfaces such as grain boundaries.[3,4] This is the case for all polycrystalline semiconductors that exhibit nonlinear conduction, the most well known being ZnO, where the effects are largest.

Grain boundaries are principally responsible for the formation of interfacial electronic states and Schottky barriers which, in principle, control the functionality of the device. It is therefore extremely important to be able to systematically and predictably engineer the properties of these grain boundaries. A key issue in this process is an understanding of the boundary properties at the microscopic level since it is here that the electronic phenomena of interest have their origin. Despite the importance of interfaces in varistor materials, surprisingly little is known about their structure. Varistor behavior and nonlinear conduction are explained in terms of phenomenological models such as the double Schottky barrier,[4] which do not specify the microscopic origin of the phenomenon. Interfacial defects or defect complexes are proposed as the cause of the observed states in the band gap, but the precise nature of these defects is unknown. It is clear that as a prerequisite to understanding how such imperfections affect the electronic properties of the material, it is necessary to obtain microscopic information concerning the interfaces at both the atomic and electronic level.

Experimentally, very few atomic resolution observations of the structure or chemistry of individual grain boundaries in TiO_2 have been reported. Exceptionally, some [010] twin[5] and [001] tilt boundaries[6,7] have been studied using high-resolution electron microscopy and atomic models for their structures have been proposed. However, no information is available on their electronic structures, primarily because of the difficulty in fabricating samples containing single grain boundaries upon which spectroscopic measurements could be made. The $\Sigma=15$ 36.9° (210)[001] tilt boundary is an example of a grain boundary whose atomic structure has been deduced experimentally.[6,7] Moreover, it has also been studied theoretically using a classical simulation approach.[6] The main characteristic of this boundary structure, which is reproduced by the simulation, is a relative translation of the two grains parallel to the boundary equal to $\sim\frac{1}{5}$[120]. The microscopy also suggests a small ($\sim$0.1 nm) contraction normal to the boundary which may be due to a local loss of oxygen or an excess of titanium ions. The classical simulation does not reproduce this effect, probably because it was performed under stoichiometric conditions. Since the atomic structure of this particular tilt boundary has been relatively well characterized, it is chosen for study using first-principles methods. The immediate aim, described in this paper, is to confirm the structural stability of the proposed atomic model and to gain some insight into its electronic structure particularly with regard to the presence and distribution of any new electronic states in the band gap. The results represent the first completely *ab initio* investigation of a grain boundary in a transition metal oxide.

II. METHOD

The calculations are based on the well-established methodology of density-functional theory in the local-density approximation (LDA) as parametrized by Perdew and Zunger,[8] combined with the pseudopotential technique.[9,10] There are extensive reviews of this method in the literature.[9] Only valence electrons are represented explicitly in the calculations, and the effects of electron exchange and correlation included in the LDA have been shown to be reliable for a wide range of materials, including oxides such as MgO. The total self-consistent ground-state energy of the system for any set of positions of the ion cores is determined using the conjugate

gradients iterative minimization technique due to Payne *et al.*[11] In this method, the total energy is minimized with respect to the plane-wave coefficients of the self-consistent occupied valence electron orbitals. The interactions between these electrons and the Ti and O cores is described by nonlocal pseudopotentials, generated by *ab initio* calculations on isolated atoms. The calculations are performed in periodic boundary conditions, with every occupied valence orbital represented as a plane-wave expansion. The expansion includes all plane waves whose kinetic energy is less than some chosen plane-wave cutoff energy. Calculations can therefore easily be taken to convergence with respect to size of basis set simply by increasing the cutoff.

The calculations were performed with the all-bands code CETEP[12] [the parallel version of the sequential code CASTEP (Ref. 11)], running on the 512-node Cray T3D machine at Edinburgh Parallel Computing Centre. The all-bands code is significantly more memory intensive than the band-by-band version of the code, but has the advantage of giving much faster electronic convergence.

Pseudopotentials for first row elements such as O, and transition metals such as Ti, need to be carefully constructed if basis-set convergence is to be achieved with a manageable number of plane waves. In the generation of these pseudopotentials, the kinetic-energy filter tuning optimization technique due to Lee *et al.*[13] has been used. Details of the pseudopotentials are as follows. The oxygen pseudopotential was generated using the reference atomic configuration $2s^2 2p^4$ for the s and p angular momentum components, and $2s^1 2p^{1.75} 3d^{0.25}$ for the d component, with core radii equal to 1.8 a.u. for the three components. For titanium we used $3d^2 4s^2$ for the s and d components, and $3d^2 4s^{0.75} 4p^{0.25}$ for the p component with core radii of 2.5 a.u. for all three components. The Kleinman-Bylander representation[14] is used for all the pseudopotentials, with the s component local for Ti, and the p component local for O. The electronic exchange and correlation energy is represented using the commonly used Ceperley-Alder form.[15] Brillouin zone sampling is performed using the Monkhorst-Pack scheme,[16] or adaptations thereof. Note that use of a plane-wave formalism allows for straightforward, accurate determination of the Hellmann-Feynman forces,[17] which can be used for *ab initio* relaxation of the ionic positions to the lowest-energy configuration. This ionic relaxation was carried out with a Broyden-Fletcher-Goldfarb-Shanno Hessian update scheme,[18] found to give convergence in a significantly smaller number of steps than conventional conjugate gradients. The relaxation continued until all the residual forces on ions were less than 0.1 eV/Å.

The grain boundary structure was relaxed using a supercell having the form shown in Fig. 1(a). It extends periodically in all directions and contains two identical, but symmetrically equivalent, $\Sigma=15$ tilt boundaries related to one another by inversion symmetry. Two different cell sizes were used: one containing 60 atoms in which the tilt boundaries are separated by 10.25 Å along [210], and one twice this size in which the boundary separation is 20.5 Å. The larger cell was used to determine the influence of boundary separation on the results. For both cells, a layer of atoms between each boundary was held crystallographically fixed in order to simulate the bulk boundary condition. The cells were held at

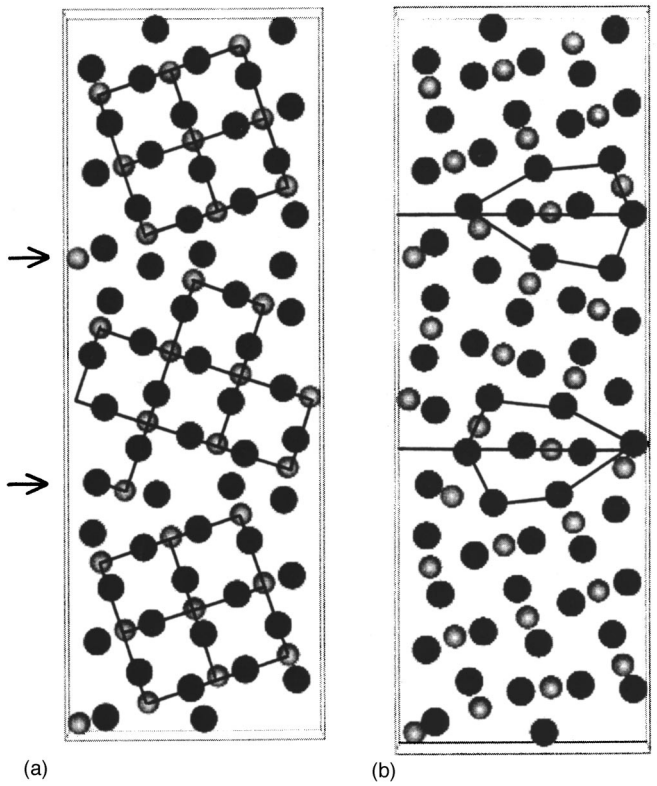

FIG. 1. (a) Atomic structure of the $\Sigma=15$ (210)[001] tilt grain boundary in TiO_2 showing the unrelaxed 60-atom supercell geometry (for clarity the figure has been extended to show more than 60 atoms). Note that the cell contains two symmetry related but equivalent grain boundaries, indicated by the arrows. The cell is viewed along [001] with Ti atoms shown light and O atoms dark. The initial unrelaxed configuration incorporates the observed in-plane translation of $\sim\frac{1}{5}$[120]. (b) The relaxed supercell geometry, showing little change from (a).

constant volume and the system was assumed to be perfectly stoichiometric. The effects of the constant volume condition is discussed in the next section. The atomic structure of the boundary at the start of the calculation was based on the one observed in the electron microscope and simulated using empirical potentials. It is characterized by a relative translation of the two grains at the boundary of $\sim\frac{1}{5}$[120]. The 60-atom cell consisted of 20 titanium and 40 oxygen atoms, amounting to 160 occupied valence bands. The larger cell had twice this number of atoms. A kinetic-energy cutoff of 500 eV was used in the calculations, corresponding to 51 200 plane waves for the larger cell. The k points $(\frac{1}{4},0,\frac{1}{4})$ and $(\frac{1}{4},0,-\frac{1}{4})$ were used for Brillouin zone sampling.

III. RESULTS AND DISCUSSION

Before starting the grain boundary calculations, the pseudopotentials were tested to determine how accurately they reproduce various bulk properties of TiO_2. In calculations using four k points and the same cutoff of 500 eV, the atomic and electronic structure of bulk rutile were determined. Table I shows that the calculated lattice parameters agree with experimental values to within approximately 2%. The band gap is of course typically underestimated within LDA, at 1.6 eV, compared to the experimental value[19] of 3

TABLE I. Comparison between experiment and the *ab initio* calculated lattice parameters and bond lengths for bulk rutile (TiO_2).

Parameter	Theory	Experiment
a (Å)	4.603	4.594
c (Å)	2.976	2.956
u	0.3039	0.3048
$\frac{c}{a}$	0.6465	0.6434
$(Ti\text{-}O)_1$ (Å)	1.961	1.949
$(Ti\text{-}O)_2$ (Å)	1.978	1.980

eV. The calculated bandwidths agree well with photoemission spectra, the error being only 5–10%.[19]

Figure 1(b), shows the 60-atom supercell after relaxation, where it is seen that the displacements away from the starting structure in Fig. 1(a) are small. An analysis of the forces remaining on the atoms, including the forces parallel to the boundary, shows that they are also small (less than 0.1 eV/Å) confirming the stability of the observed translation state of the boundary. Furthermore, the sum of the forces parallel to the grain boundary on the atoms that were held fixed is approximately zero, indicating a minimum with respect to translation. This sum is significantly smaller than the forces on the individual atoms. This stability is not affected by using a larger supercell and, indeed, all the structural and energetic characteristics of the boundary calculated with the small cell are confirmed when the larger cell is employed.

To illustrate this we have determined the differential displacements normal to the boundary of the atomic layers after relaxation for both cell sizes. These displacements were calculated by subtracting the starting atomic positions normal to the boundary from the normal positions in the final crystallographic configuration. Figure 2 compares the form and magnitude of these displacements, where it is seen that the maximum displacements occur in the immediate vicinity of the boundary (labeled by an arrow) and are almost the same for the 60- and 120-atom models. This is the case for both the titanium and oxygen sublattices; for clarity the figure shows only the oxygen sublattice. In addition, the variation of these displacements with respect to distance away from the boundary is also very similar for both model sizes. This variation is characterized by alternating positive and negative displacements, which fall off rapidly from the boundary. Thus, we are confident that our use of a 60-atom supercell does not impose a major constraint on the relaxation. Moreover, by doubling the cell size we have shown that the constant volume condition is also not a serious limitation since the grain boundary structure remains essentially the same. In particular, the local volume change at each boundary for both cell sizes is estimated to be 0.05 nm, which is similar to the classical value of 0.04 nm obtained[6,7] under constant pressure conditions. This gives a total volume change of order 0.1 nm for two grain boundaries. We would expect a quantum mechanical constant pressure calculation to produce a similar result but have not attempted such a calculation here since it is more computationally demanding and would require determination of the Pulay stress.[20] There spurious internal stresses are a result of the finite number of

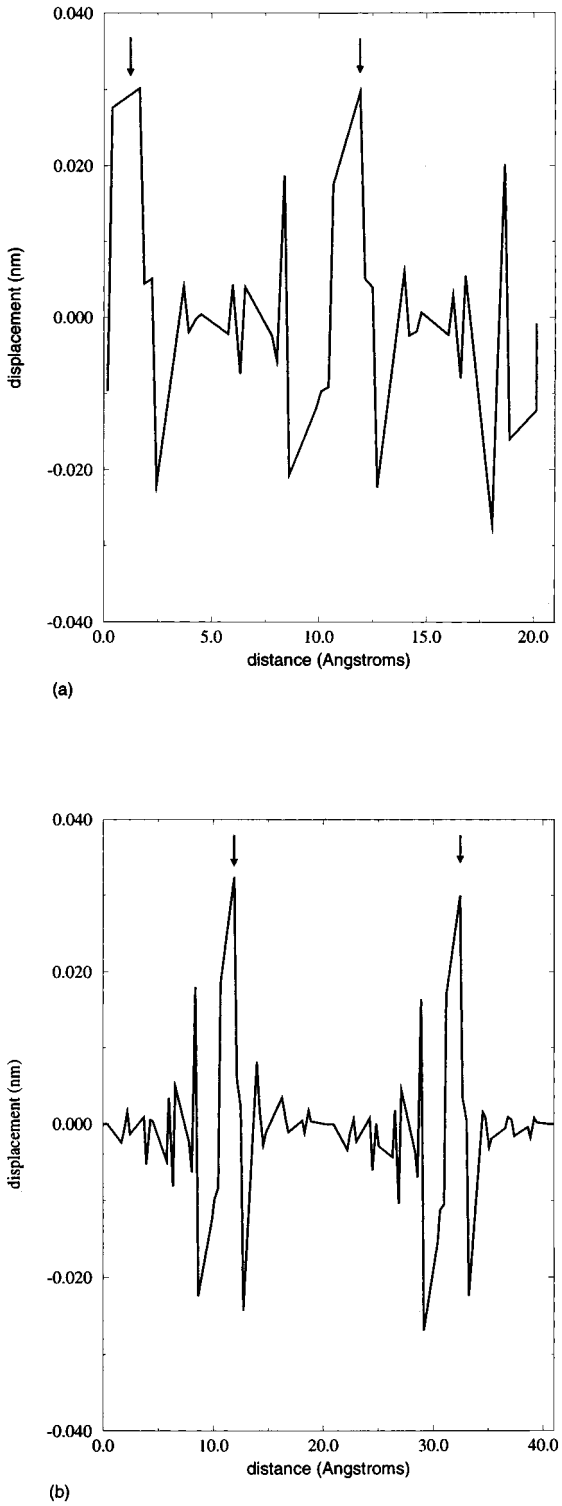

FIG. 2. Differential displacements normal to the boundary plane of the oxygen sublattice atomic layers for (a) the 60-atom model and (b) the 120-atom model. The arrows indicate the locations of the two boundaries in the models. Note the difference in the horizontal scales for (a) and (b).

basis states used in the calculations. The experimental observation of a boundary contraction is most likely to be caused by the presence of point defects in the boundary as mentioned earlier. Since we are satisfied with the reliability of the 60-atom supercell, most of the results presented here will

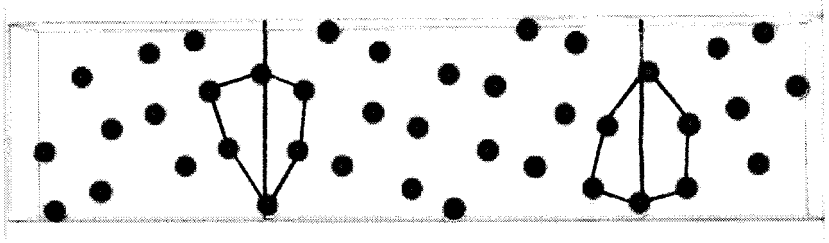

FIG. 3. Relaxed atomic structure of the $\Sigma=15$ tilt boundary in the 120-atom supercell showing only the oxygen sublattice in the $z=0$ plane. The 'kite' shaped structural units illustrate the equivalence of the two boundaries in the cell and the mirror symmetry across each boundary plane.

focus on that system and reference will only be made to the larger cell to show when the differences are small.

The symmetry of the oxygen sublattice at the tilt boundary is indicated in Fig. 1(b) by the kite-shaped structural units. It is seen that this sublattice is mirror symmetric across the boundary ensuring that the oxygen bond distortion is minimized. This is new structural information that is not derived from the electron microscope observations since these observations were made under conditions in which the oxygen ions are not imaged. The relaxed boundary configuration thus removes the mirror symmetry of the titanium sublattice (by the in-plane translation) but conserves the mirror symmetry of the oxygen sublattice. The symmetry of the oxygen sublattice is further highlighted in Fig. 3 where, for the large supercell, only the oxygen ions have been displayed. Figure 4 illustrates the distribution of (Ti-O) bonds in the relaxed small supercell. In bulk TiO_2, there are two sets of (Ti-O) bonds: those of length 1.96 and 1.98 Å. In the tilt boundary region, the bond lengths vary from between 1.81 and 2.03 Å (i.e., -6% to $+2\%$ of the bulk values). The oxygen octahedra in the boundary core, also shown in Fig. 4, are correspondingly distorted.

Figure 5 displays a shaded contour plot of the calculated pseudocharge density on a (001) plane passing through Ti and O sites for the relaxed 60-atom supercell. A similar plot for the 120-atom supercell is shown in Fig. 6. Such plots are useful in understanding exactly how the bonding at grain boundaries differs from bonding in the bulk. The identification of regions of increased electron density may be useful in understanding phenomena such as segregation to grain boundaries and diffusion along grain boundaries. Notice that in the bulk region between the two grain boundaries (more easily identified in the large supercell), the charge density is highly localized on the oxygen ions and is nearly spherically symmetric. Since this is a pseudopotential calculation, only the valence electron density is shown. The highly ionic nature of the material means that the valence electron density is concentrated almost entirely on oxygen sites and the titanium ions are invisible. However, there is certainly non-negligible covalent bonding present in the bulk and there seems to be an even greater degree of covalency in the boundary core. This is illustrated by the small flares of charge density located along the [110] (Ti-O) bond directions. Thus, as expected, the structural properties of TiO_2 in the bulk or near a defect cannot be completely described by a fully ionic model. The covalent nature of the (Ti-O) bond has been noted before in previous experimental and theoretical studies.[19] The distribution of charge density about the grain boundary plane is not completely mirror symmetric due to the influence of the titanium sublattice, which is not seen in these plots but is translated along the boundary.

Since some of the bonds are distorted in the relaxed tilt boundary structure, electronic states should be present in the band gap. We therefore expect the boundary to have some intrinsic electrical activity which, if significant, would have

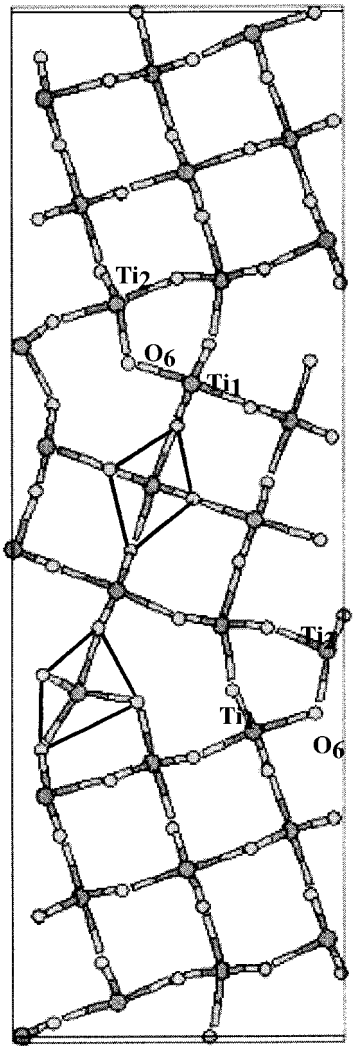

FIG. 4. Atomic structure of the $\Sigma=15$ tilt boundary in the 60-atom supercell illustrating the Ti-O bonds and the distortion of the oxygen octahedra in the boundary core. The labels Ti^1, Ti^2, and O^6 refer to undercoordinated atoms also shown in Fig. 9.

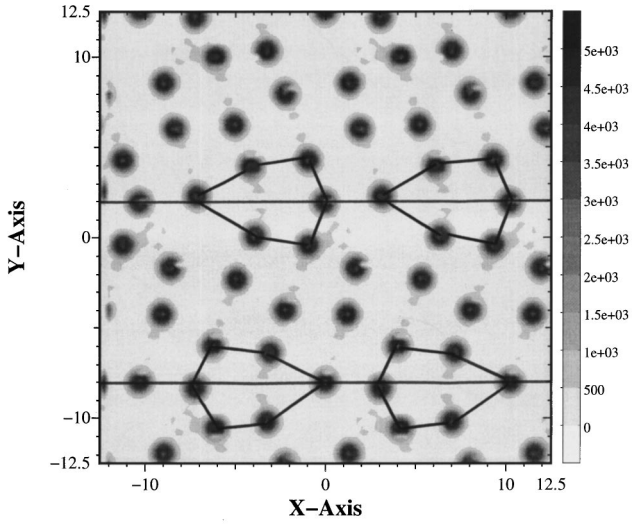

FIG. 5. Calculated valence charge-density distribution through a (001) section of the 60-atom supercell passing normal to each boundary. The x and y axes are along [120] and [210], respectively. The electron density varies from approximately zero in the light areas to about 4.5 electrons per cubic Å in the dark areas. Most of the electron density is concentrated on the oxygen sites and is spherically symmetric. Observe the mirror symmetry of the oxygen sublattice across each grain boundary plane.

important consequences for device applications as described earlier. To determine the presence of grain boundary interface states, the electronic Kohn-Sham eigenvalues of the relaxed ionic configuration have been calculated at the $(\frac{1}{4}, 0, \frac{1}{4})$ k point. Figure 7 shows the total normalized valence-band density of states for bulk TiO_2 and the 60-atom grain boundary supercell. The top of the valence band and bottom of the conduction band in the bulk are located at -2.9 and -0.3 eV, respectively. The peaks at -19.0 and -5.0 eV correspond to the O-2s band and hybridized O-2p/Ti-3d band. The calculated total density of states for the grain boundary model is seen to have similar characteristics to that of the

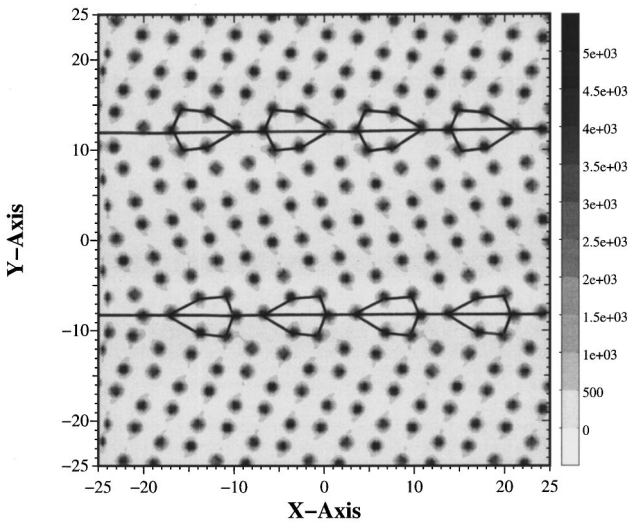

FIG. 6. Calculated valence charge-density distribution through a (001) section of the 120-atom supercell showing few differences compared to the smaller supercell.

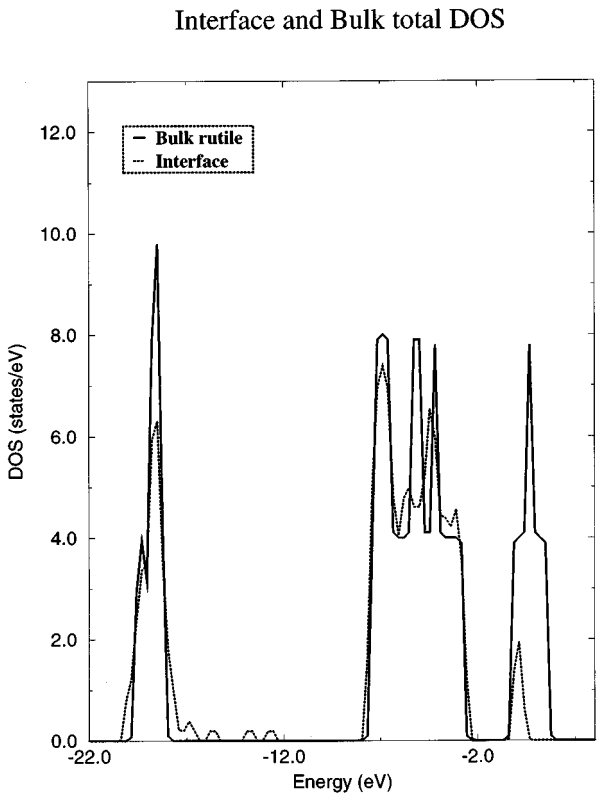

FIG. 7. Total normalized valence band density of states (DOS) at $(\frac{1}{4},0,\frac{1}{4})$ for bulk rutile and the relaxed 60-atom supercell. Note the increased bandwidth in the boundary system. This is consistent with the overall trend towards bond length reduction in the boundary core. A decrease in bond length means that the atoms are pushed closer together, i.e., there is greater orbital overlap than in the bulk, hence a larger bandwidth. The band gap is from -2.9 to -0.3 eV.

bulk, i.e., the peak positions remain at roughly the same energies, suggesting no major change in the bonding. The only major difference, for both the 60- and 120-atom models, is that several localized filled states extend into the band gap from the valence-band edge. This is as expected because of the bond length and bond angle distortions inherent in the grain boundary core region. The states extending into the band gap are distributed between -2.89 and -2.72 eV and are too small to be seen on the scale of this figure. There are no deep levels introduced into the fundamental band gap consistent with this boundary being of low energy and having a reasonably well-coordinated structure. The valence-band density of states (DOS) for the large model has almost exactly the same characteristics as the 60-atom model, apart from the loss of some features near the top edge of the O-2s band, most likely arising from interaction between the two interfaces in the small model. In all other respects the 60-atom and 120-atom DOS are the same. The calculated boundary energy was found to be 1.91 J m^{-2} for the small supercell and 1.72 J m^{-2} for the large model. Clearly the larger boundary energy found for the small cell indicates that a certain level of interaction does exist between the two boundaries contained in the small model. The large cell boundary energy is quite close to the classical value of 1.70 J m^{-2}.[6]

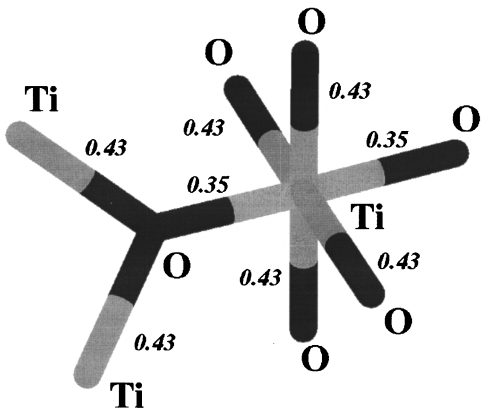

FIG. 8. Bond populations of bulk TiO_2 bonds.

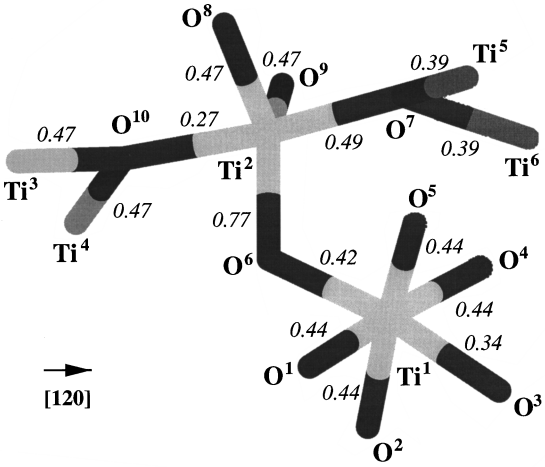

FIG. 9. Bond populations in the boundary core region showing the effect of bond order alternation. The orientation of the boundary plane is approximately horizontal.

A Mulliken population analysis[21] of the plane-wave pseudopotential calculations has been performed on both bulk TiO_2 and the 120-atom grain boundary supercell. This is done using a scheme described in Ref. 22, to project the plane-wave eigenfunctions onto a linear combination of atomic orbitals basis set.[23] The projection technique calculates the density matrix $P_{\mu\nu}(\mathbf{k})$ and the overlap matrix $S_{\mu\nu}(\mathbf{k})$ of the atomic basis set, which are sufficient to perform population analysis of the electronic distribution. The Mulliken charge associated with a given atom A is given in this scheme by

$$Q_m(A)=\sum_{\mathbf{k}}(w_{\mathbf{k}})\sum_{\mu}^{onA}\sum_{\nu}P_{\mu\nu}(\mathbf{k})S_{\mu\nu}(\mathbf{k}) \qquad (1)$$

and the overlap population (bond order) between two atoms A and B by

$$n_m(AB)=\sum_{\mathbf{k}}(w_{\mathbf{k}})\sum_{\mu}^{onA}\sum_{\nu}^{onB}2P_{\mu\nu}(\mathbf{k})S_{\mu\nu}(\mathbf{k}). \qquad (2)$$

In both of these equations $w_{\mathbf{k}}$ are the weights associated with the k points in the Brillouin zone. The bond population is indicative of the strength of the bond between a pair of atoms A and B.

Figures 8 and 9 show the results of the analysis for both the perfect bulk system and a section of the interface in the 120-atom cell. The quality of the projection of the plane-wave eigenstates is assessed by the calculation of a spilling parameter. This is zero when the projected wave functions perfectly represent the plane-wave states, and 1 when the atomic basis set is orthogonal to the plane-wave eigenstates. In both calculations this parameter was of order 0.001, sufficiently small for our purposes. In the bulk it is found that each Ti atom, which is sixfold coordinated, has a Mulliken charge of $+1.45$ electrons, and each O atom is threefold coordinated with a Mulliken charge of -0.73 electrons. The two sets of (Ti-O) bonds have bond populations of 0.35 and 0.43 electrons, respectively. In the interface core region, oxygens are found with only twofold coordination. One of these is shown labelled O^6 in Fig. 9. In order to maintain the same total bond population as a bulk O, it forms a particularly strong bond (population 0.77) with a nearby Ti atom, labelled Ti^2. This Ti^2 atom is found to be only fivefold coordinated. The twofold coordinated O^6 has a Mulliken charge of -0.59, and the corresponding fivefold coordinated Ti^2 has a Mulliken charge of $+1.31$. These changes are due to the reduction in coordination of these atoms.

The (Ti^2-O^6) bond is strengthened at the expense of the (Ti^2-O^{10}) bond, which is significantly weakened, with a population of only 0.27 electrons. In order to maintain the total bond population of the fivefold coordinated Ti^2 the bond population of the (Ti^2-O^8) bond is found to be increased, in a similar manner to that of the twofold coordinated O^6. The changes in the strengths of these bonds have a knock-on effect as we move along the boundary. The (Ti^3-O^{10}) and (Ti^4-O^{10}) bonds are found to be strengthened while the (Ti^5-O^7) and (Ti^6-O^7) bonds are found to be weakened. This charge transfer effect is known as bond-order alternation.

IV. CONCLUSIONS

Our finding that the $\Sigma=15$ 36.9° (210)[001] tilt boundary introduces localized shallow states mainly associated with the upper edge of the valence band and no deep states in the band gap is consistent with the computational results of others on similar well-coordinated tilt boundaries in alumina,[24] germanium,[25] and silicon.[26] It suggests that these types of boundary structures may not in themselves be responsible for the observed electronic properties of polycrystalline semiconducting oxides. Grain boundary defects, such as impurities and vacancies, have been proposed as a major contributor to these properties. Having established the microscopic characteristics of a clean defect-free boundary, further work is now in progress to examine the influence of point defects and impurities in the boundary.

ACKNOWLEDGMENTS

I.D. acknowledges support from EPSRC. This work was supported by EPSRC Grants Nos. GR/K03975 and GR/K41649. The latter provided an allocation of time on the Cray T3D 512-node parallel machine at Edinburgh Parallel

Computing Centre, U.K. Thanks are also due to Ruben Perez and Rajiv Shah for useful discussions. M.D.S. would like to thank Rajiv Shah and Chris Pickard for their help in the development of the population analysis codes and acknowledges the funding of M.L. Laboratories plc. P.D.B. acknowledges fruitful discussions with the oxide interface group at M.I.T., and Molecular Simulations Inc. for the provision of CERIUS2.

*Present address: Department of Physics, Tamkang University, Tamsui, Taipei, 25137, Taiwan.

[1] K. S. Koto, *Solid State Electrochemistry and its Applications to Sensors and Electronic Devices* (Elsevier, New York, 1988).

[2] *Ceramic Materials for Electronics*, edited by R. C. Buchanan (Marcel Dekker, New York, 1991).

[3] *Grain Boundaries in Semiconductors*, edited by H. Leamy, G. Pike, and C. Seager, MRS Symposia Proceedings No. 5 (Materials Research Society, Pittsburgh, 1982).

[4] L. Hozer, *Semiconductor Ceramics: Grain Boundary Effects* (Ellis Harwood, New York, 1994).

[5] W.-Y. Lee, P. D. Bristowe, Y. Gao, and K. L. Merkle, Philos. Mag. Lett. **68**, 309 (1993).

[6] W.-Y. Lee, P. D. Bristowe, I. G. Solorzano, and J. B. Vandersande, in *Defect-Interface Interactions*, edited by E. P. Kvam, A. H. King, M. J. Mills, T. D. Sands, and V. Vitek, MRS Symposia Proceedings No. 319 (Materials Research Society, Pittsburgh, 1994), p. 239.

[7] U. Dahmen, S. Paciornik, I. G. Solorzano, and J. B. Vandersande, Inter. Sci. **2**, 125 (1994).

[8] P. Perdew and A. Zunger, Phys. Rev. B **16**, 5188 (1976).

[9] G. P. Srivastava and D. Weaire, Adv. Phys. **36**, 463 (1987).

[10] M. J. Gillan, in *Computer Simulation in Materials Science*, Vol. 205 of *NATO Advanced Study Institute, Series E: Applied Science*, edited by M. Mayer and V. Pontikis (Kluwer, Dordrecht, 1991), p. 257.

[11] M. C. Payne, M. P. Teter, D. C. Allan, T. A. Arias, and J. D. Joannopoulos, Rev. Mod. Phys. **64**, 1045 (1992).

[12] L. J. Clarke, I. Štich, and M. C. Payne, Comput. Phys. Commun. **72**, 14 (1992).

[13] M.-H. Lee, J. S. Lin, M. C. Payne, V. Heine, V. Milman, and S. Crampin, Phys. Rev. B (to be published).

[14] L. Kleinman and D. M. Bylander, Phys. Rev. Lett. **48**, 1425 (1982).

[15] D. M. Ceperley and B. J. Alder, Phys. Rev. Lett. **45**, 566 (1980).

[16] H. J. Monkhorst and J. D. Pack, Phys. Rev. B **13**, 5188 (1976).

[17] R. P. Feynman, Phys. Rev. **56**, 340 (1939).

[18] W. H. Press, B. P. Flannery, S. A. Teukolsky, and W. T. Vetterling, *Numerical Recipes: The Art of Scientific Computing* (Cambridge University Press, Cambridge, 1989).

[19] K. M. Glassford and J. R. Chelikowsky, Phys. Rev. B **46**, 1284 (1992).

[20] P. Pulay, Mol. Phys. **17**, 197 (1967).

[21] R. S. Mulliken, J. Chem. Phys. **23**, 1833 (1955).

[22] D. Sanchez-Portal, E. Artacho, and J. M. Soler, Solid State Commun. **95**, 685 (1995).

[23] M. D. Segall, C. J. Pickard, R. Shah, and M. C. Payne, Mol. Phys. (to be published).

[24] S.-D. Mo, W. Y. Ching, and R. H. French, J. Am. Ceram. Soc. **79** 627 (1996).

[25] E. Tarnow, T. Arias, P. D. Bristowe, P. Dallot, G. P. Francis, J. D. Joannopoulos, and M. C. Payne, in *Atomic Scale Calculations of Structure in Materials*, edited by M. S. Daw and M. A. Schluter, MRS Symposia Proceedings No. 193 (Materials Research Society, Pittsburgh, 1990), p. 235.

[26] M. Kohyama, R. Yamamoto, Y. Ebata, and M. Kinoshita, J. Phys. C. **21**, 3205 (1988).